ANALYTICAL SCIENCES JANUARY 2010, VOL. 26

Redox Cycling Effect on the Surface-enhanced Raman Scattering Signal of Crystal Violet Molecules at Nanostructured Interdigitated Array Electrodes

Md. Monirul ISLAM,* Kosei UENO,*, and Hiroaki MISAWA*†**

**Research Institute for Electronic Science, Hokkaido University, Sapporo 001-0021, Japan*
***PRESTO, Japan Science and Technology Agency, Kawaguchi 332-0012, Japan*

Nanostructured interdigitated array (IDA) electrodes with different inter-electrode spacing were demonstrated to improve the detection sensitivity of short-lived electroactive species and to follow interfacial dynamics by their surface-enhanced Raman scattering (SERS) functionality. Nanostructured IDA electrodes fabricated using electron beam lithography were used for an electrochemical SERS study of irreversible electroactive species, crystal violet (CV), in an aqueous KCl solution in single and generation-collection (GC) mode experiments. The GC mode enabled us to amplify the SERS intensity. An inter-electrode spacing dependent study found the maximum number of redox cycling, collection efficiency and amplification of the SERS intensity. Its SERS function disclosed the potential-dependent dynamics of CV molecules at the electrode surface, which was not observed in the redox current. Miniaturized nanostructured IDA electrodes are of great importance for developing lab on chip devices, and are useful for analyzing dynamical features within small space/volume domains, which require small amounts and/or concentration of analytes.

(Received November 26, 2009; Accepted December 10, 2009; Published January 10, 2010)

Introduction

Microelectrodes and their arrays[1] are promising for investigating the electrochemical processes of mechanistic and/or analytical interest[2,3] because of their high mass-transport rates.[4] The miniaturized sizes of these devices have been exploited in many applications, such as lab-on-a-chip systems,[5-9] a scanning electrochemical microscope (SECM),[10] analysis in a single biological cell[11] and so on. The interdigitated array (IDA) electrode involves one of the most effective structures to improve the sensitivity in detecting electroactive species through a redox cycling mechanism.[12-16] Although their use offers many advantages, non-Faradic interfacial events, such as adsorption, desorption and potential-induced structural orientations can rarely be displayed because these processes yield nearly non-measurable currents. In contrast, surface-enhanced Raman scattering (SERS)[17] is very sensitive to these processes. Thus, the development of IDA electrodes consisting of metallic nanostructures required for SERS functionality extends their applicability for monitoring the dynamics of electrode-electrolyte interfaces. In addition, nanostructured IDA electrodes with definitive nano-gap feature-sizes capable of enhancing electric fields, particularly at the nano-gap positions,[18,19] can be employed to handle the intricate electrochemistry problems, for instance, the excited states or structural transition proceeded in multi-photon perturbation, photo-energy conversion and so on. It is known that a narrower gap between the electrode bands results in the higher sensitivity.[13,20] Nanostructured IDA electrodes with a narrower inter-electrode spacing are effective for detecting short-lived electroactive species and following the kinetics and dynamics of quasi-reversible or irreversible electrochemical reactions because the reactive or unstable products/intermediates can be collected to the adjacent electrodes before dissociation into other stable products, or involved in secondary homogeneous chemical reactions. Recently, we have developed[21] nanostructured IDA electrodes with SERS functionality using a high-precision electron beam lithography (EBL) combination with a lift-off technique, and successfully applied to an electrochemical SERS study of a ferri/ferrocyanide system in aqueous $KClO_4$. The results showed a strong correlation between the number of redox cycling and the collection efficiency derived from the redox current and the SERS intensity, respectively. This paper describes an electrochemical SERS study of irreversible or quasi-reversible redox species, namely crystal violet (CV) molecules in an aqueous KCl solution as a function of the inter-electrode spacing and the dynamics at an electrode-electrolyte interface. The variation of the inter-electrode spacing enabled us to set up the optimized band distant for obtaining maximum redox cycling, collection efficiency and SERS amplification. The amplification of the SERS intensity in the generation-collection mode was explained while considering the potential-induced orientations, electrochemical reduction, replacement of CV molecules by reduced product at the collector electrode and the redox cycling/feedback mechanism.

Experimental

Materials and apparatus

Glass substrates (24 × 24-mm-square and 0.5-mm-thick) were purchased from Matsunami, Ltd. Japan for electrode fabrication.

† To whom correspondence should be addressed.
E-mail: misawa@es.hokudai.ac.jp

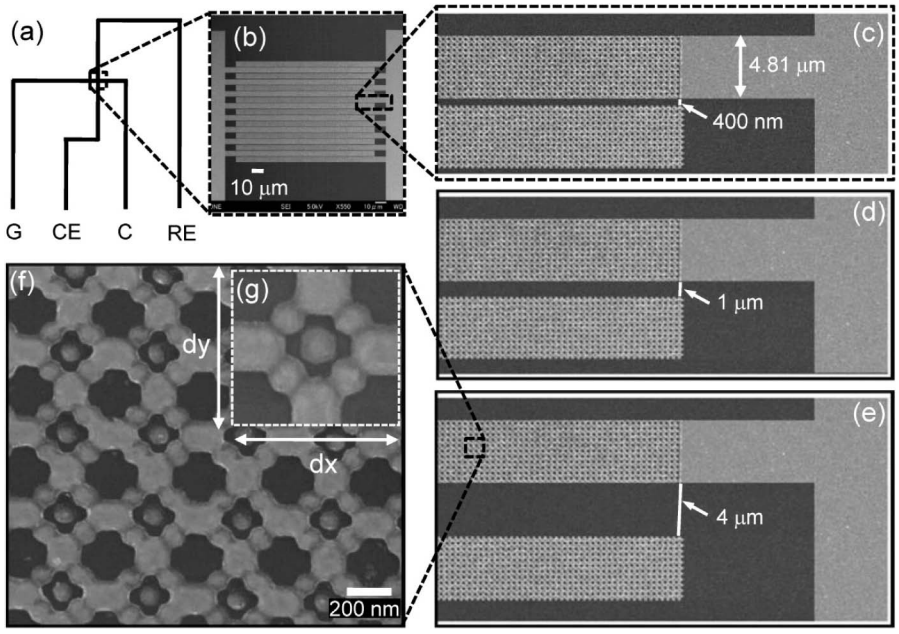

Fig. 1 Schematic representation of nanostructured IDA electrodes: RE, CE and G & C, respectively, refer to reference, counter and working electrodes of Au. (a) Layout; (b) low magnification SEM image; (c) – (e) SEM images at different inter-electrode band distances; (f) high magnification SEM image exploring the nano-patterns; (g) a base unit, dx = dy = 350 nm.

A positive-type electron beam resist, ZEP-520A, resist developer ZEP-N50 (*n*-amyl acetate), rinse solution, ZMD (methyl isobutylketone, 89; isopropyl alcohol, 11%), resist remover and ZDMAC (dimethylacetamide) were procured from Zeon Co., Ltd., Tokyo, Japan. Acetone and methanol obtained from Wako Pure Chemical Industries, Ltd. were used for substrate cleaning and metal lift-off using ultrasonic water baths. Sputter targets Au (99.99%) and Cr (99.99%) were purchased from Kojundo Chemical Lab. Co., Ltd. for depositing Cr/Au bilayers by ultra high-vacuum helicon sputter (MPS-4000, ULVAC Technologies Inc., Japan). A positive photo-resist, OFPR-5000 from Tokyo Ohka Kogyo Co., Ltd., Tokyo, Japan and a negative photo-resist, SU8-2002 from MicroChem Inc., were used to fabricate large electrode pads and insulator film, respectively. A field-emission scanning electron microscope (FE-SEM, JSM-6700FT, JEOL) was used for characterizing the electrode surface. Crystal violet (99.5%) and KCl were purchased from Wako Pure Chemical Industries, Ltd., and water was purified through a Milli-Q system (Millipore). The potentials of electrochemical SERS measurements were controlled by a dual potentiometer (ALS Model 832a, BAS Inc., Tokyo, Japan). SERS measurements were acquired through a 100× magnification water-immersion objective lens of numerical aperture NA = 0.75 (LMPlanFL, Olympus) by a microscope (BX51, Olympus). A near-IR laser diode (λ = 785 nm) was used for sample irradiation, and SERS spectra were collected on an Acton SP300i (Princeton Instruments) imaging spectrometer equipped with a charged couple device (CCD) camera cooled at –100°C by liquid nitrogen.

Electrode fabrication

Nanostructured IDA electrodes were fabricated onto a glass substrate using high-resolution EBL, UV photolithography, ultra-high vacuum sputtering and lift-off, and large bonding pads and insulator layers by the conventional photolithography. The details of electrode fabrication are reported elsewhere.[19,21,22] The design, layout and SEM images of the electrodes are shown in Fig. 1. The electrode arrays were made of 17 band-electrodes of Au; the dimensions of each were 100 μm-long and 4.81 μm-wide with various inter-electrode band distances (0.4, 0.7, 1.0, 2.0, 4.0 μm). On a smaller scale, the bands consisted of $94 \times 94 \times 40$ nm^3 Au nanoblocks, blocks, with four nanoblocks arranged around the central nanoblock along diagonals (Fig. 1g) forming a pattern consisting of five nanoblocks in total. The nanogaps were formed between central and four neighboring nanoblocks, which, in turn, were electrically interconnected with the connector nanoblocks ($100 \times 100 \times 40$ nm^3) into the nanostructured IDA electrode. The nanogaps generated between vertexes of nanoblocks are those particular locations where local field enhancement takes place and optical linear as well as nonlinear effects are enhanced. It has been reported[21] that the fabricated electrodes show two optical extinction peaks at λ_1 = 595 nm and λ_2 = 784 nm into water with a strong electric-field enhancement (~10^4 times relative to incident light), particularly at the nanogap positions.

Electrochemical SERS measurements

The spectroelectrochemical cell for Raman-scattering experiments was made by connecting the bonding edges of printed nanostructured IDA electrodes on a glass plate placed on an optically transparent polystyrene stage. Cu lead wires were attached strongly to bonding edges by Ag paste and an epoxy resin adhesive. A 2×10^{-4} mol dm^{-3} CV in 0.1 mol dm^{-3} KCl aqueous solution was used for measurements of the electrochemical SERS responses at fabricated nanostructured IDA electrodes. G and C electrodes fabricated at different inter-electrode spacing (Fig. 1a) were used as working electrodes, whereas RE and CE, respectively, reference and counter electrode fabricated onto the same glass plate. Measurements of the current responses and SERS spectra were performed in single (S) and generation-collection (GC) mode experiments using an amperometric technique. The potential of

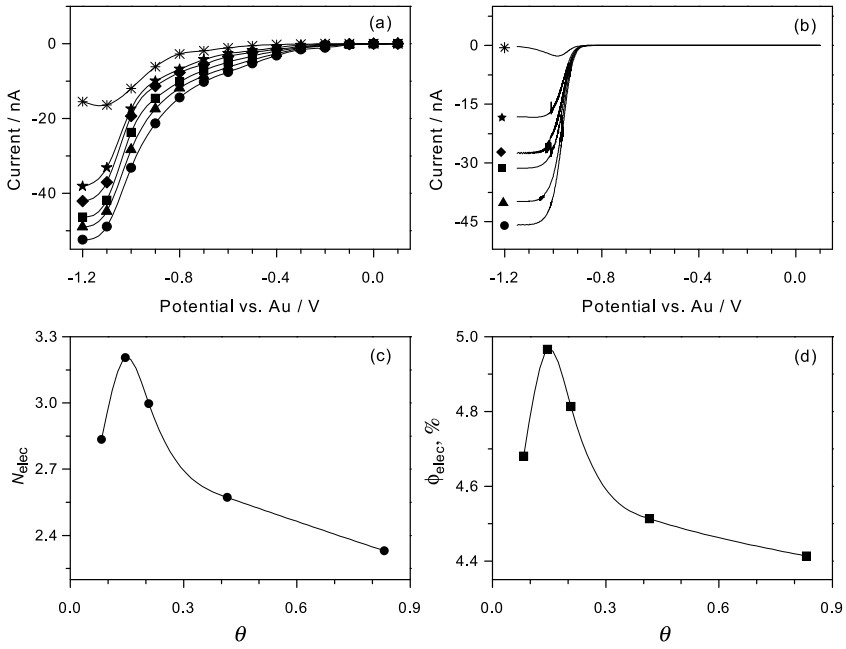

Fig. 2 (a) Cathodic current at the G electrodes using 2×10^{-4} mol dm^{-3} aqueous CV molecules in 0.1 mol dm^{-3} KCl; (b) the cathodic current at the G electrode by an FEM simulation in the S mode (✳) and the GC mode at different inter-electrode spacings (■, 400 nm; ●, 700 nm; ▲, 1 μm; ◆, 2 μm; ★, 4 μm); (c) and (d), respectively, are the number of redox cycling, N_{elec}, and collection efficiency, ϕ_{elec}% as a function of θ (= α/β, α is the inter-electrode spacing and β the electrode band width).

the G electrode was varied from 0.1 to –1.2 V in both the S and GC mode experiments and the C electrode used in only the GC mode was kept at 0.1 V. The G electrode played the role of a generator electrode and C for the collector electrode. All SERS measurements were carried out under a slightly de-focused condition in order to avoid any damage to the nanostructures due to absorption heating. Each spectrum was collected by irradiating typical 5 mW laser power with a spectral integration time of 15 s and at a spectral resolution of less than 3 cm^{-1}. All potential values were controlled relative to a reference Au electrode incorporated onto a nanostructured IDA electrode plate.

Results and Discussion

Electrochemical properties

The cathodic responses of 2×10^{-4} mol dm^{-3} CV in 0.1 mol dm^{-3} KCl aqueous solutions to the G electrode as a function of the applied potential and the inter-electrode spacing (α) are summarized in Fig. 2a. It can be observed from Fig. 2a that the current at the G electrode increased by a small slope as the potential was shifted to the negative direction from the initial potential, 0.1 to –0.8 V, and then rapidly increased to the limiting value at around –1.2 V. A slow increase of the cathodic current in the 0.1 to –0.8 V potential region was due to molecular re-orientation[23] of the crystal violet molecules, supporting electrolytes and solvent molecules as the charge state of the electrode surface changed due to a potential perturbation. The rapid increase region was caused by a reduction of the crystal violet *via* a one-electron transfer mechanism. The current derivative to the applied potential, *i.e.*, d*i*/d*E*, showed a maximum at –1.0 V, corresponding to the reduction potential of the crystal violet, which coincided with an earlier reported[23] value, –0.6 V *vs*. SCE (since under the experimental condition, the potential of Au was measured to be 0.39 V *vs*. SCE). In the S mode, the reduction current showed a peak at around –1.1 V due to diffusion-limited electron transfer kinetics. However, in the GC mode, the reduction current attained the limiting values due to an ample mass transfer to the electrode surface through spherical/hemi-spherical diffusion of the analyte molecules, facilitated by a redox cycling mechanism. To better understand the experimental results and redox cycling mechanism, numerical simulations of the electrochemical responses were performed on the basis of a finite element method (FEM) by using a computer software package (PDEase 2D, Macsyma Inc.). The simulation model had better accuracy for the reversible electroactive species applied in this study.[24] The simulation results shown in Fig. 2b revealed a small deviation from the experimentally observed current-potential curves because of an underestimate of the irreversible electrochemical behavior of CV molecules. In spite of a quantitative mismatch between simulation and experimental results, it could amply explain the experimental current-potential curves qualitatively.

The increase in the G electrode currents and the anodic responses of the C electrode in the GC mode were reflected in the number of redox cycling and the collection efficiency. The number of redox cycling was calculated using the relation:[25] $N_{elec} = G_{GC}/G_S$, and the collection efficiency from $\phi_{elec}\% = 100 \times C_{GC}/G_{GC}$, where G_{GC} and C_{GC} are the limiting current at the G and C electrode, respectively, in the GC mode; G_S is the limiting current at the G electrode in the S mode. The experimental N_{elec} and ϕ_{elec} are presented in Figs. 2c and 2d, respectively, as a function of a dimensionless parameter, $\theta = \alpha/\beta$, where α is the inter-electrode spacing and β the electrode band width. The N_{elec} *vs*. θ and ϕ_{elec} *vs*. θ curves showed well-defined maxima at a θ value corresponding to 700 nm inter-electrode spacing, and attained maximum values of ~3.2 and ~5%, respectively. The maxima at this inter-electrode spacing are attributed to non-interacting diffusion profiles and

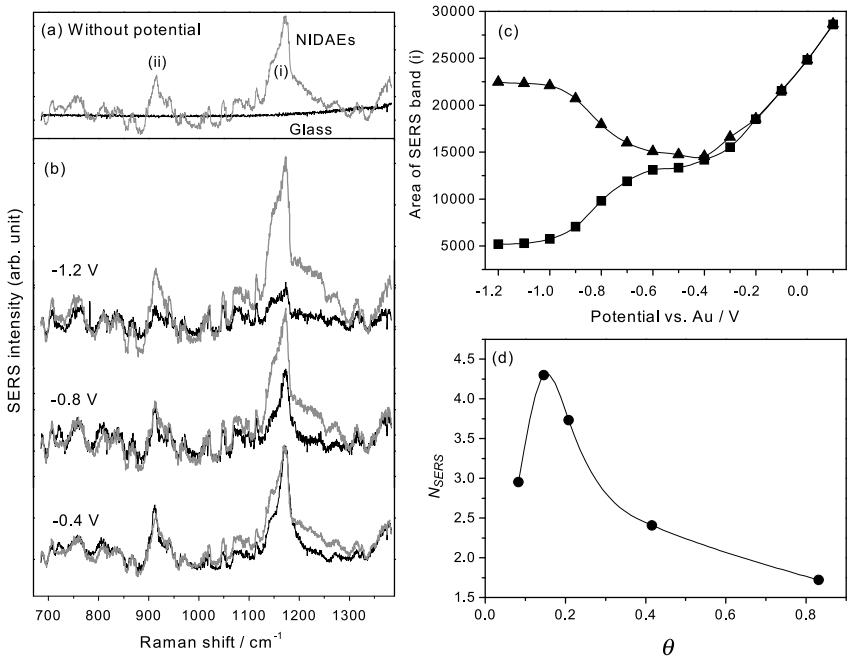

Fig. 3 (a) SERS spectra of 2×10^{-4} mol dm^{-3} CV molecules in 0.1 mol dm^{-3} KCl aqueous solutions without a potential at the glass (black) and nanostructured IDA electrodes (gray); (b) comparative SERS spectra between the S (black) and GC (gray) modes, measured at different potentials using a G electrode of 700 nm inter-electrode spacing; (c) integrated SERS intensity of band (i) as a function of the applied potential in the S mode (■) and the GC mode (▲); (d) number of the redox cycling, N_{SERS}, calculated from the integrated SERS band intensity as a function of θ (= α/β, α is inter-electrode spacing and β the electrode band width).

no shielding effect[14] of the G and C electrodes to each other ensuring maximum mass transfer rate to both of the electrodes. On the other hand, for a 400-nm inter-electrode spacing, the diffusion layer at the G electrode sprayed over and partially shielded the surface of neighboring C electrode causing lower N_{elec} and ϕ_{elec} values. Since the diffusion fluxes to the electrode surface is inversely related to the thickness of the diffusion layer and at the higher inter-electrode spacing (1, 2 and 4 μm), the electrodes will experience lower mass transfer effects, and thus a lower values of N_{elec} and ϕ_{elec}. In addition, the life-time of the electro-generated species may be very short compared to the diffusion time-laps at a higher inter-electrode spacing, causing a rapid decrease of both N_{elec} and ϕ_{elec}. It is important to mention that the observed value of ϕ_{elec} is so small that one would expect larger to be relevant for corresponding N_{elec} value. The observed anomalies in ϕ_{elec} are due to differences in the orientation of CV molecules to the electrode surface. The origin of the anomalous behavior is discussed in a later section.

Potential and inter-electrode spacing dependent SERS signals

Fabricated nanostructured IDA electrodes were used to measure SERS responses of a 2×10^{-4} mol dm^{-3} aqueous solution of CV including 0.1 mol dm^{-3} KCl as a supporting electrolyte. The normal Raman and SERS spectra of CV were measured by dispersing a few drops of solution onto a glass substrate and nanostructured IDA electrodes, respectively, and irradiating by a 785-nm laser source with a typical power of 5 mW for a 15-s integration time. These are shown in Fig. 3a. In the studied spectral range, the glass surface did not show any characteristics bands associated with CV molecules, while at nanostructured IDA electrodes the SERS spectrum of CV exhibited two strong bands at (i) 1173 cm^{-1} and (ii) 909 cm^{-1}. Band (i) was assigned to the in-plane ring C–H bending vibration,[26,27] and band (ii) to the ring skeletal vibration of the radial orientation.[28] The appearance of strong bands in the SERS spectrum demonstrates that the light field enhancement at the nano-gaps where the light field was strong facilitated SERS detection of low-concentration CV molecules on the fabricated nanostructured IDA electrodes with gold nanostructures.

For a detail investigation of the potential and inter-electrode spacing-dependent SERS responses of CV molecules to fabricated nanostructured IDA electrodes, the SERS spectra were collected in S and GC mode experiments at a potential interval of 0.1 V, starting from 0.1 to –1.2 V. Comparative SERS spectra measured at –0.4, –0.8 and –1.2 V in the S and GC modes using nanostructured IDA electrodes of 700 nm inter-electrode spacing are shown in Fig. 3b. It is apparent that the intensity of the SERS band at –1.2 V amplified the manifold in the GC mode. The area of band (i) was calculated, and is represented in Fig. 3c as a function of the applied potential. It is discernible from this figure that the SERS band intensity in both modes decreased rapidly in the region from 0.1 to –0.4 V. At a more negative potential region from –0.8 to –1.0 V, it decreased to the minimum in the S mode, while in the GC mode it increased rapidly to a limiting value. The SERS at the electrode caused secondary effects, such as adsorption, desorption, electrochemical reactions of the pre-surface species and the diffusion of solution species towards the electrode surface.[29] It is well known that a high-light intensity field attracts and dipole-orients optically polarized molecules.[30] The behavior of the observed SERS band intensity against the applied potential can be rationalized by considering the potential of zero charge (PZC) at the electrode surface, the orientation and the reduction of CV molecules, the redox cycling mechanism

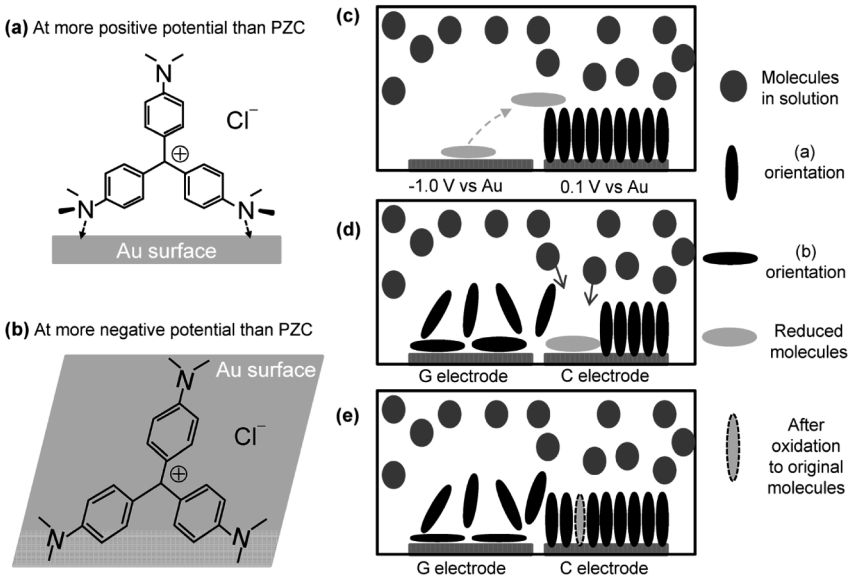

Fig. 4 A schematic representation of the orientation of CV molecules to Au-surface and mechanism behind the amplification of the SERS intensity in the GC mode: (a) perpendicular orientation; (b) flat orientation; (c) reduction of CV molecules at the G electrode and diffusion to the C electrode; (d) replacement of CV molecules by reduced molecules at the C electrode and diffusion of replaced CV molecules to the G electrode; (e) perpendicular orientation of reduced molecule at the C electrode after oxidation to CV molecules and occupation of relaxed surface by the molecules diffused from the bulk solution.

and the volume of diffusion layers. The PZC value depends on the methods applied for the determination, the cleanness of the surface and the crystal faces of electrode materials. The reported[31–37] PZC of the Au-electrode (single crystal faces or polycrystalline) in an aqueous KCl solution was observed within the range from 0.33 to –0.5 V *vs*. SCE. The potential-dependent SERS intensity revealed that the PZC of the nanostructured Au-electrode in 2×10^{-4} mol dm^{-3} CV molecules including 0.1 mol dm^{-3} KCl is located around –0.4 V *vs*. Au. The positive charged surface favors a perpendicular orientation (Fig. 4a) of CV molecules to Au-surface through the lone-pair electrons of N-atoms in p-substituted -N(CH$_3$)$_2$ moieties. As the potential is shifted to the negative direction, the perpendicular orientation is disfavored by a growing negative charge at the Au surface due to an electrostatic repulsion between the negative electrode surface and the electron cloud of N atoms in the p-substituted -N(CH$_3$)$_2$ moieties. As a result, this orientation flipped to a flat orientation, as shown in Fig. 4b, where CV molecules are oriented to the Au surface through positive π-molecular orbital lying parallel to molecular plane. Thus, the rapid decrease in the SERS band intensity in the potential region from 0.1 to –0.4 V account for the change in the orientation of CV molecules from perpendicular to flat. Since a flat orientation is suitable for electron transfer from the Au-electrode to the positive π-molecular orbital, it facilitated the reduction of CV molecules. Therefore, a rapid fall of the SERS intensity in the more negative potential region from –0.8 to –1.0 V is attributed to a reduction of CV molecules *via* a one-electron transfer step. Afterwards, the radial or spherical mass transport to the electrode surface established a quasi-steady SERS intensity.

The SERS intensity of CV molecules in the GC mode within –0.6 to –1.2 V is higher than that at the potential (~–0.6 V) where the reduction of CV molecules commenced. Recently, we have reported[21] a potential and redox cycling dependent SERS of the ferri/ferrocyanide reversible redox couple at similar nanostructured IDA electrodes, where the SERS intensity in the GC mode was higher than that in the S mode at the negative end of the applied potential, but was not observed to exceed the value of the initial potential. The number of the redox cycling and collection efficiency calculated from the SERS intensity was in accordance to that it was calculated from the electrochemical currents, and the amplification of the SERS intensity attributed to a redox cycling mechanism. In this study, the redox cycling number calculated from the SERS intensity (N_{SERS}), which is shown in Fig. 3d as a function of θ, is larger than the N_{elec} values. However, the intriguingly amplification of the SERS intensity and the N_{SERS} value in the GC mode can be explained not only by considering the redox cycling mechanism but also the potential-dependent orientation of CV molecules to the Au surface, which is schematically illustrated in Fig. 4. Since the C electrode was kept at 0.1 V more positive than PZC, where a large number of profoundly perpendicular orientated CV molecules were replaced by a single molecule of reduced product of flat oriented CV molecules to G electrode (Fig. 4c) because its oxidation to the original one at the C electrode also favored a flat orientation (Fig. 4d). After oxidation, its flat orientation reverted to being perpendicular at the C electrode, and empty surface was produced in a revert orientation occupied by diffused molecules from the bulk solution (Fig. 4e). Thus, the oxidation of a single reduced product of CV molecules at the C electrode supplied a multiple number of original CV molecules to the G electrode and thereby extra amplification of SERS intensity in the GC mode. Note that a small amount of reduced molecules reached to the C electrode because of their short lifetime, giving rise to a small figure of the C electrode current, and hence a low collection efficiency. It is important to mention that the ferricyanide ion belongs to the octahedral symmetry, and all of its possible orientations to the electrode surface at all applied potential occupy the same area, which accounts for agreements concerning the electrochemical and

SERS behaviors. The potential-dependent SERS and current curve showed some different characteristics; for example, the current was almost constant from the initial potential to –0.8 V, while the SERS intensity exhibited a transition at PZC. Because the structural orientation to the electrode surface is a non-Faradic process, the current change in this process is extremely small, and its contribution to the observed current is negligible. On the other hand, the SERS intensity is strongly influenced by the orientation of molecules to the electrode surface, and the molecular orientation to the electrode surface was observed to be reflected in the potential-dependent SERS band intensity. The GC mode using irreversible redox moieties reflected deeper insights into the orientation of CV molecules to the electrode surface, and the amplified SERS intensity to a large extent.

Conclusions

The nanostructured IDA electrodes with SERS functionality at different inter-electrode spacing were successfully fabricated, and were used to investigate electrochemical SERS responses of crystal violet molecules in S and GC mode experiments. The GC mode showed an extra-ordinary amplification of the SERS intensity due to a redox cycling accomplished with the potential-induced orientation of CV molecules to the electrode surface. An inter-electrode spacing dependent study enabled us to find the maximum redox cycling number, collection efficiency and amplification of SERS intensity in the GC mode. The SERS functionality of developed nanostructured IDA electrodes with narrower inter-electrode spacing explored the electrode-electrolytes interfacial dynamics of CV molecules, which was unrevealed in the electrochemical properties. It offers a new opportunity to improve not only the analytical sensitivity, but also the detection ability of short-lived electroactive species and in monitoring the interfacial dynamics.

Acknowledgements

This work was supported by funding from the Ministry of Education, Culture, Sports, Science, and Technology of Japan: KAKENHI, Grant-in-Aid for Scientific Research on the Priority Area “Strong Photon-Molecule Coupling Fields” (No. 470 (No. 19049001)) and 20710068, Grants-in-Aid from Hokkaido Innovation through Nanotechnology Support (HINTS), Monbukagakusho Scholarship for foreign students support, and Global Center of Excellence (GCOE) through Graduate School of Information Science and Technology, Hokkaido University, Japan.

References

1. O. Ordeig, F. J. Campo del, F. J. Munoz, C. E. Banks, and R. G. Compton, *Electroanalysis*, **2007**, *19*, 1973.
2. K. Stulik, C. Amatore, K. Holub, V. Marecek, and W. Kutner, *Pure Appl. Chem*., **2000**, *72*, 1483.
3. C. Amatore, “*Physical Electrochemistry*”, ed. I. Rubinstein, **1995**, Chap. 4, New York, Marcel Dekker, 131.
4. C. S. Henry and I. Fritsch, *J. Electrochem. Soc*., **1999**, *143*, 3367.
5. M. Morita, O. Niwa, and T. Horiuchi, *Electrochim. Acta*, **1997**, *42*, 3177.
6. W. R. Vandaveer, D. J. Woodward, and I. Fritsch, *Electrochim. Acta*, **2003**, *48*, 3341.
7. E. Nebling, T. Grunwald, J. Albers, P. Schäfer, and R. Hintsche, *Anal. Chem*., **2004**, *76*, 689.
8. Z. Liu, O. Niwa, R. Kurita, and T. Horiuchi, *Anal. Chem*., **2000**, *72*, 1315.
9. A. J. Bard, F. R. F. Fan, J. Kwak, and O. Lev, *Anal. Chem*., **1989**, *61*, 132.
10. G. Justin, S. Finley, A. R. A. Rahman, and A. Guiseppi-Elie, *Biomed. Microdevices*, **2009**, *11*, 103.
11. K. L. Adams, M. Puchades, and A. G. Ewing, *Annu. Rev. Anal. Chem*., **2008**, *1*, 329.
12. D. G. Sanderson and L. B. Anderson, *J. Am. Chem. Soc*., **1985**, *57*, 2388.
13. O. Niwa, M. Morita, and H. Tabei, *Electroanalysis*, **1991**, *3*, 163; (b) O. Niwa, M. Morita, and H. Tabei, *Anal. Chem*., **1990**, *62*, 447; (c) O. Niwa, M. Morita, and H. Tabei, *J. Electroanal. Chem*., **1989**, *267*, 291.
14. A. J. Bard, J. A. Crayston, G. P. Kittlesen, T. V. Shea, and M. S. Wrighton, *Anal. Chem*., **1986**, *58*, 2321.
15. U. Wollenberger, M. Paeschke, and R. Hintsche, *Analyst*, **1994**, *119*, 1245.
16. E. D. Goluch, B. Wolfrum, P. S. Singh, M. A. G. Zevenbergen, and S. G. Lemay, *Anal. Bioanal. Chem*., **2009**, *394*, 447.
17. D. L. Jeanmaire and R. P. Van Duyne, *J. Electroanal. Chem*., **1977**, *84*, 1.
18. K. Ueno, V. Mizeikis, S. Juodkazis, K. Sasaki, and H. Misawa, *Opt. Lett*., **2005**, *30*, 2158.
19. K. Ueno, S. Juodkazis, V. Mizeikis, K. Sasaki, and H. Misawa, *Adv. Mater*., **2008**, *20*, 26.
20. A. E. Cohen and R. R. Kunz, *Sens. Actuators*, **2000**, *62*, 23.
21. M. M. Islam, K. Ueno, S. Joudkazis, Y. Yokota, and H. Misawa, *Anal. Sci*., **2010**, *26*, 13.
22. K. Ueno, S. Juodkazis, T. Shibuya, Y. Yokota, V. Mizeikis, K. Sasaki, and H. Misawa, *J. Am. Chem. Soc*., **2008**, *130*, 6928.
23. R. C. Kaye and H. I. Stonehill, *J. Chem. Soc*., **1952**, 3231.
24. K. Ueno, H.-B. Kim, and N. Kitamura, *Anal. Chem*., **2003**, *75*, 2086.
25. K. Ueno, M. Hayashida, J.-Y. Ye, and H. Misawa, *Electrochem. Commun*., **2005**, *7*, 161.
26. I. Persaud and W. E. L. Grossman, *J. Raman Spectrosc*., **1993**, *24*, 107.
27. M. V. Canamares, C. Chenal, R. L. Birke, and J. R. Lombardi, *J. Phys. Chem. C*, **2008**, *112*, 20295.
28. S. Sunder and H. J. Bernstein, *Can. J. Chem*., **1981**, *59*, 964.
29. T. Watanabe and B. Pettinger, *Chem. Phys. Lett*., **1982**, *89*, 501.
30. Y. Nabetani, H. Yoshikawa, A. C. Grimsdale, K. Mullen, and H. Masuhara, *Langmuir*, **2007**, *23*, 6725.
31. T. R. Beck, *J. Phys. Chem*., **1969**, *73*, 466.
32. R. A. Fredlein, A. Damjanovic, and J. O. M. Bockris, *Surf. Sci*., **1971**, *25*, 261.
33. R. A. Fredlein and J. O. M. Bockris, *Surf. Sci*., **1974**, *46*, 641.
34. A. Hameline, *J. Electroanal. Chem*., **1995**, *386*, 1.
35. S. J. O’Shea, M. E. Welland, T. A. Brunt, A. R. Ramadan, and T. Rayment, *J. Vac. Sci. Technol., B*, **1996**, *14*, 1383.
36. R. Raiteri and H. J. Butt, *J. Phys. Chem*., **1996**, *99*, 15728.
37. J. Lipkowski, *Can. J. Chem*., **1999**, *77*, 1163.